INTER-SCALE TRANSFER OF PASSIVE SCALAR IN GRID TURBULENCE

Muyang Wang
Department of Mechanical Systems Engineering
Nagoya University
Furocho, Chikusa-ku, Nagoya 464-8603, Japan
wang.muyang.k9@s.mail.nagoya-u.ac.jp

Takuya Yurikusa
Department of Mechanical Systems Engineering
Nagoya University
Furocho, Chikusa-ku, Nagoya 464-8603, Japan
tyurikusa@i.softbank.jp

Koji Iwano
Department of Mechanical Systems Engineering
Nagoya University
Furocho, Chikusa-ku, Nagoya 464-8603, Japan
iwano@nagoya-u.jp

Yasuhiko Sakai
Nagoya Industrial Science Research Institute
Sakae, Naka-ku, Nagoya 464-0008, Japan
ysakai@mech.nagoya-u.ac.jp

Yasumasa Ito
Department of Mechanical Systems Engineering
Nagoya University
Furocho, Chikusa-ku, Nagoya 464-8603, Japan
yito@nagoya-u.jp

ABSTRACT

Direct numerical simulations were carried out to study the turbulence generated by a regular square grid. Two-point correlation analysis using the scale-by-scale scalar (SBSS) equation and the third-order structure function was applied to reveal the mechanism of inter-scale scalar transport. The results show that the scalar displays a trend of inverse cascade in the vertical direction at the scale that is larger than the integral length scale.

INTRODUCTION

Since the first experiments of (Simmons & Salter, 1934), the turbulent motion behind a grid has been investigated intensively in many experiments and numerical simulations. In general, the turbulent flow behind the grid can be roughly classified into two regions: the developing region that wakes interact each other and are significantly affected by structures of grids, and the developed region in the downstream area that has quasi-homogeneous isotropic features. This difference between upstream and downstream promotes the understanding of the development and evolution of turbulence. Therefore, many researchers have recently conducted a series of studies focusing on the extreme event, intermittency and self-preservation on the upstream and downstream region.

On the other hand, the Karman-Howarth-Monin-Hill (KHMH) equation shown by Eq. 1 represents the inter-scale energy transfer between two spatial points $\mathbf{x}$ and $\mathbf{x}'$, and it has been widely used to investigate the mechanism in various situations (Gomes-Fernandes *et al.*, 2015; Portela *et al.*, 2017; Zhou *et al.*, 2020).

$$
\begin{aligned}
&\underbrace{\frac{\partial\langle\delta q^2\rangle}{\partial t}}_{4A_t}+\underbrace{\left(\frac{U_j+U_j'}{2}\right)\frac{\partial\langle\delta q^2\rangle}{\partial X_j}}_{4A}+\underbrace{\frac{\partial\langle\delta u_j\delta q^2\rangle}{\partial r_j}}_{4\Pi}+\underbrace{\frac{\partial\delta U_j\langle\delta q^2\rangle}{\partial r_j}}_{4\Pi_U}\\
&=\underbrace{-\frac{2}{\rho}\frac{\partial\langle\delta u_j\delta p\rangle}{\partial X_j}}_{4T_p}\underbrace{-2\langle\delta u_i\delta u_j\rangle\frac{\partial\delta U_i}{\partial r_j}-\langle\left(u_j+u_j'\right)\delta u_i\rangle\frac{\partial\delta U_i}{\partial X_j}}_{4P}\\
&\underbrace{-\frac{\partial}{\partial X_j}\left(\frac{\langle\left(u_j+u_j'\right)\delta q^2\rangle}{2}\right)}_{4T_u}+\nu\left[\underbrace{2\frac{\partial^2}{\partial r_j^2}}_{4D_\nu}+\underbrace{\frac{1}{2}\frac{\partial^2}{\partial X_j^2}}_{4D_{X,\nu}}\right]\langle\delta q^2\rangle\\
&\underbrace{-2\nu\left[\langle\left(\frac{\partial u_i}{\partial x_j}^2\right)\rangle+\langle\left(\frac{\partial u_i'}{\partial x_j'}^2\right)\rangle\right]}_{4\varepsilon}
\end{aligned}
\tag{1}
$$

Here, $\delta q^2=\delta u_i^2$, $\delta U_i=U_i-U_i'$ and $\delta p=p-p'$. The angle bracket $\langle\cdot\rangle$ means the ensemble average, U_i refers to the i component of mean velocity vector, and u_i indicates the i component of the fluctuation of velocity vector, p is the pressure, respectively. The symbol δ represents a difference of the physical properties between the spatial location $\mathbf{x}=\mathbf{X}+\mathbf{r}/2$ and $\mathbf{x}'=\mathbf{X}-\mathbf{r}/2$, where $\mathbf{X}$ is the centroid of two different points $\mathbf{x}$ and $\mathbf{x}'$, $\mathbf{r}$ is the distance between the two points.

Similar to the energy transfer, the scale-by-scale scalar transport can be expressed as in Eq. 2 using the second-order structure function (Hill, 2002):

$$
\begin{aligned}
&\underbrace{\frac{\partial\langle\delta c^2\rangle}{\partial t}}_{4A_{t,c}}+\underbrace{\left(\frac{U_j+U_j'}{2}\right)\frac{\partial\langle\delta c^2\rangle}{\partial X_j}}_{4A_c}+\underbrace{\frac{\partial\langle\delta u_j\delta c^2\rangle}{\partial r_j}}_{4\Pi_c}+\underbrace{\frac{\partial\delta U_j\langle\delta c^2\rangle}{\partial r_j}}_{4\Pi_{U,c}}\\
&=\underbrace{-2\langle\delta c\delta u_j\rangle\frac{\partial\delta C}{\partial r_j}-\langle\left(u_j+u_j'\right)\delta c\rangle\frac{\partial\delta C}{\partial X_j}}_{4P_c}\\
&\underbrace{-\frac{\partial}{\partial X_j}\left(\frac{\langle\left(u_j+u_j'\right)\delta c^2\rangle}{2}\right)}_{4T_c}+\nu\left[\underbrace{2\frac{\partial^2}{\partial r_j^2}}_{4D_\kappa}+\underbrace{\frac{1}{2}\frac{\partial^2}{\partial X_j^2}}_{4D_{X,\kappa}}\right]\langle\delta c^2\rangle\\
&\underbrace{-2\kappa\left[\langle\left(\frac{\partial c}{\partial x_j}^2\right)\rangle+\langle\left(\frac{\partial c'}{\partial x_j'}^2\right)\rangle\right]}_{4\chi}
\end{aligned}
\tag{2}
$$

where C refers to the mean scalar , c indicates the fluctuation of scalar, and $\delta C = C - C'$ and $\delta c = c - c'$. This equation is also known as the scale-by-scale scalar transfer budget equation (SBSS equation). In Eq. 2, A_c represents the advection of δc^2 by the mean flow, Π_c is the non-linear transfer term, $\Pi_{U,c}$ is the linear transfer terms, P_c is the turbulent production, T_c is turbulent transport terms, D_κ is molecular diffusion in $\mathbf{r}$ space, $D_{X,\kappa}$ is the molecular diffusion along X, and χ is scalar dissipation, $A_{t,c}$ is time dependence terms. While there are many studies on energy transfer, analysis for the scalar transfer is relatively limited. Therefore, the main object of this paper is set to investigate the transport mechanism for scalar in the regular grid-generated turbulence with different Reynolds numbers and at streamwise positions.

It has been widely used to investigate the mechanism in various flows (Yasuda & Vassilicos, 2018; Zhou *et al.*, 2020). A similar discussion can be made for scalar by extending the equation proposed by (Hill, 2002), although analysis for the scalar transfer is relatively rare. Therefore, the main objective of the present research was set to investigate the inter-scale transport mechanism for scalar in grid-generated turbulence.

NUMERICAL METHODS

In this study, direct numerical simulations (DNSs) are performed. Figure 1 shows the schematic view of the computational domain. It is a rectangular box with $L_x \times L_y \times L_z = 32M \times 6M \times 6M$, where M is the distance between two grid bars. The inlet Reynolds number based on the inlet velocity U_0 and the length of grid bar M, Re_M, is set to $5,000, 9,000$, and $15,000$. The resolution calculated by $\Delta x/\eta$ does not exceed 2, where Δx is the computational mesh size and η is the Kolmogorov scale. The statistical results are collected over $100,000$ time steps with an interval of $\Delta t = 3.5 \times 10^{-4}$ after the flow reach the steady state. The initial courant number is set to 0.3.

The governing equations are the dimensionless Navier-Stokes equation, the equation of continuity and the scalar transport equation. The Schmidt number S_c is set to 1. The flow field is solved using the finite difference method with the fractional step method. The Poisson equation is solved by the conjugate gradient (CG) method. The explicit/implicit hybrid scheme based on the third-order Runge–Kutta method and the Crank–Nicolson method is applied for time integration. The periodic condition is employed in the vertical (y) and spanwise (z) direction for velocity and scalar. The advective outflow condition for the velocity and scalar field is adopted at the outlet. The inlet condition of velocity is a uniform stream of $U_0 = 1.0$, while the scalar is set to two parallel streams of $C_0 = 0.0$ and $C_1 = 1.0$.

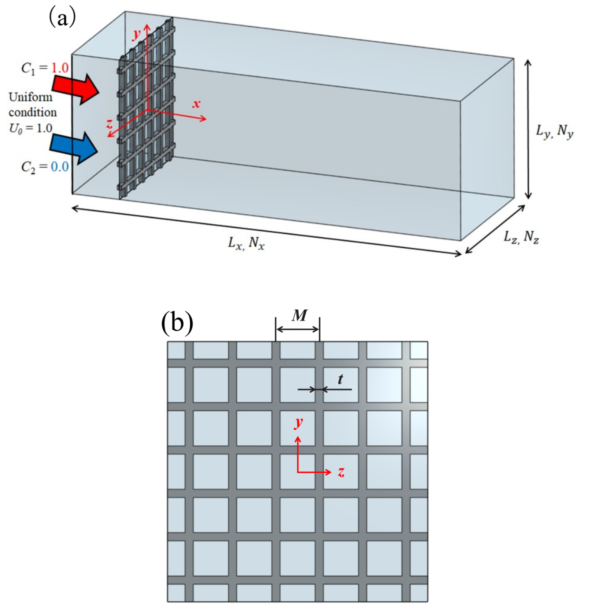

Figure 1. Schematic view of (a) the computational domain and (b) the turbulence-generating grid.

RESULTS AND DISCUSSION

Figures 2-4 show the distributions of the terms in the SBSS equation for different Re_M, respectively. Recent Studies (Obligado & Vassilicos (2019); Meldi & Vassilicos (2021)) mentioned that the tendency towards equilibrium for inter-scale energy transfer presents only in the vincity of the Taylor micro scale λ, and there is a systematic departure from equilibrium as the scale r are considered further away from λ. Since the form of the SBSS equation is similar to KHMH equation, the equilibrium and non-equilibrium characteristics of the inter-scale scalar transport may have similar behavior. Hence, the Taylor microscale λ is also employed when normalizing the relative position r between two-points $\mathbf{x}$ and $\mathbf{x}'$ in x coordinate. On the other hand, the y coordinate represents the terms normalized by χ^a, where the upper index a indicates the circumferential average. As illustrated by Figs. 2-4, the molecular diffusion D_κ^a balances the dissipation χ^a at the scale close to $r = 0$ regardless of the streamwise position and the Re_M, while other terms are almost zero. This is similar to the energy transfer, in which conversion from kinetic energy to thermal energy plays the main role when the scale is small. Additionally, since there is a mean scalar gradient in the vertical direction, the production term P_c^a is large for large r. Meanwhile, the non-linear transfer term Π_c^a reaches a peak around $r/\lambda = 1$ in all cases. Negative value of Π_c^a, which indicates an inverse cascade of the non-linear scalar transport, is observed in some cases, while others do not show such behavior.

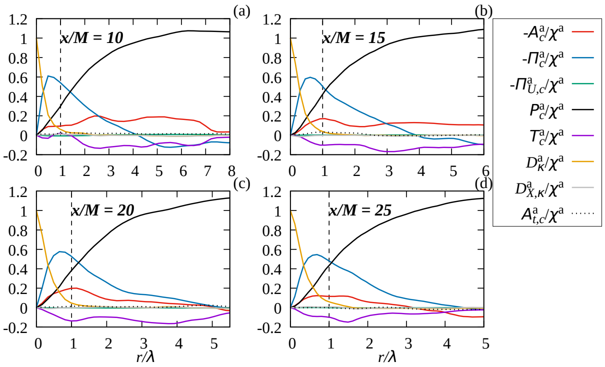

Figure 2. Circumferentially averaged terms in SBSS equation normalized by the averaged scalar dissipation rate χ^a at (a)$x/M = 10$, (b)$x/M = 15$, (c)$x/M = 20$, and (d)$x/M = 25$ in case of $Re_M = 5{,}000$.

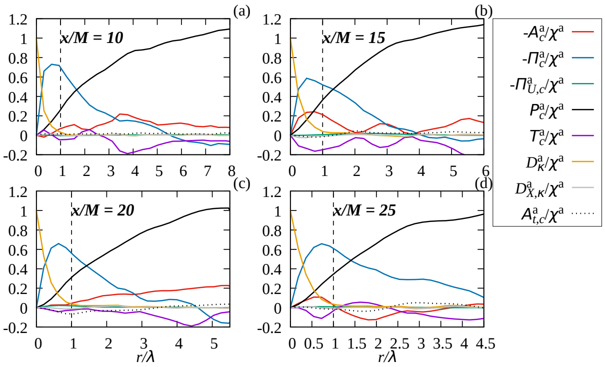

Figure 3. Circumferentially averaged terms in SBSS equation normalized by the averaged scalar dissipation rate χ^a at (a)$x/M = 10$, (b)$x/M = 15$, (c)$x/M = 20$, and (d)$x/M = 25$ in case of $Re_M = 9{,}000$.

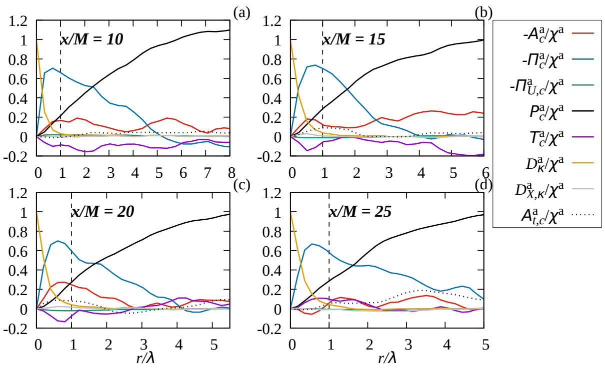

Figure 4. Circumferentially averaged terms in SBSS equation normalized by the averaged scalar dissipation rate χ^a at (a)$x/M = 10$, (b)$x/M = 15$, (c)$x/M = 20$, and (d)$x/M = 25$ in case of $Re_M = 15{,}000$.

To make this clearer, comparisons of Π_c^a with different Re_M in the developing region ($x/M = 10$) and developed region ($x/M = 25$) were conducted. Figure 5 shows the results. The evolution of $-\Pi_c^a/\chi^a$ is subjected to Re_M. With the increase of Re_M, $-\Pi_c^a/\chi^a$ tends to take a negative value at relatively large r/λ regardless the streamwise positions, indicating that the minimum scale of the inverse cascade phenomenon becomes larger for larger Re_M. This also implies

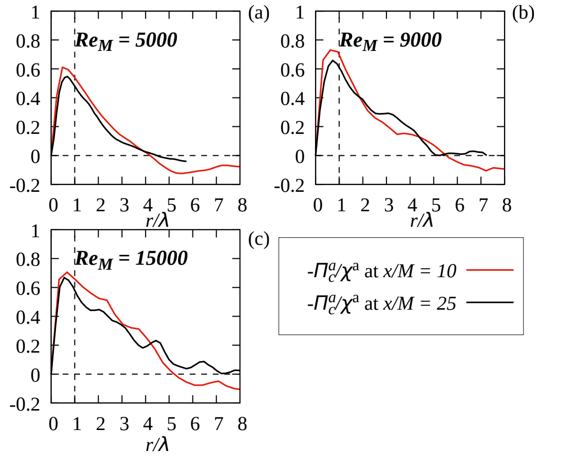

Figure 5. The evolution of the normalized non-linear transfer terms $-\Pi_c/\chi^a$ at different positions in cases of (a) $Re_M = 5{,}000$, (b) $Re_M = 9{,}000$ and (c) $Re_M = 15{,}000$.

that the high turbulent intensity restrains the process of scalar transport from small scale to large scale. Furthermore, the difference of Π_c^a between the developing region and developed region become more significant with the increase of the Re_M.

For the sake of investigating the mechanism behind this phenomenon, the third-order structure functions are introduced here to quantify the transport between different scales, as shown in Eq. 3,

$$\begin{aligned} \langle \delta u_\parallel \delta q^2 \rangle &= \langle (u_\parallel(x) - u_\parallel(x'))\,(u_i(x) - u_i(x'))^2 \rangle \\ \langle \delta u_\parallel \delta c^2 \rangle &= \langle (u_\parallel(x) - u_\parallel(x'))\,(c(x) - c(x'))^2 \rangle . \end{aligned} \tag{3}$$

The third-order structure function for energy is also ploted for a comapasion. Here the subscript $||$ denotes the component of the velocity vector parallel to the separation vector $\mathbf{r}$. Also, a schematic view of the coordinates to express the function is shown in Fig. 6.

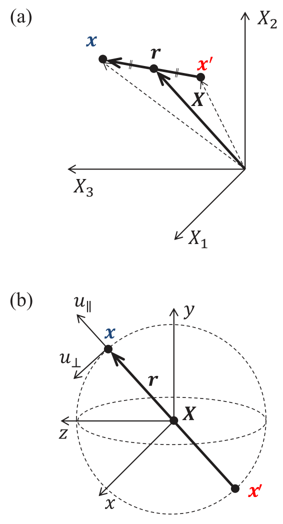

Figure 6. Schematic view of (a) the two points coordinate system(b) the decomposition of the velocity vector.

When energy or scalar transports from large scale to small scale, the radial velocity difference $\delta u_{||}$ achieves a negative value. Thus, positive sign of $-\langle \delta u_{||}\delta q^2\rangle$ represents a normal cascade and it is the inverse cascade when its sign is negative. The distribution of circumferentially averaged third-order structure functions over r for energy and scalar are shown in Figs. 7 and 8, respectively. These figures reveal that both the third-order structure functions for energy and scalar reach a peak at around $r/\lambda = 1$. However, the inverse cascade of the scalar is observed for all cases, while almost only the normal cascade is observed for energy except the upstream region ($x/M = 10$). A possible reason causing this difference is the difference of inflow conditions between velocity and scalar. Therefore, a decomposition of Π_c was conducted:

$$
\begin{aligned}
-\Pi_c &= -\frac{\partial}{\partial r_j}\langle \delta u_j \delta c^2\rangle \\
&= -\frac{\partial}{\partial r_x}\langle \delta u \delta c^2\rangle - \frac{\partial}{\partial r_x}\langle \delta v \delta c^2\rangle - \frac{\partial}{\partial r_z}\langle \delta w \delta c^2\rangle \\
-\Pi_{cx} &= -\frac{\partial}{\partial r_x}\langle \delta u \delta c^2\rangle \\
-\Pi_{cy} &= -\frac{\partial}{\partial r_y}\langle \delta v \delta c^2\rangle \\
-\Pi_{cz} &= -\frac{\partial}{\partial r_z}\langle \delta w \delta c^2\rangle
\end{aligned} \tag{4}
$$

The expressions of the components of Π_c^a in three directions are shown in Eq. (4). Figure 9 displays the distributions at the upstream region of $x/M = 10$ are displayed in Fig. 9. Both the x and z components gradually decrease for $r > \lambda$ and eventually converge to 0, while the y component decreases rapidly and takes negative values after reaching the peak. In other words, it is found that Π_{cy} causes the inverse cascade pheonmenon.

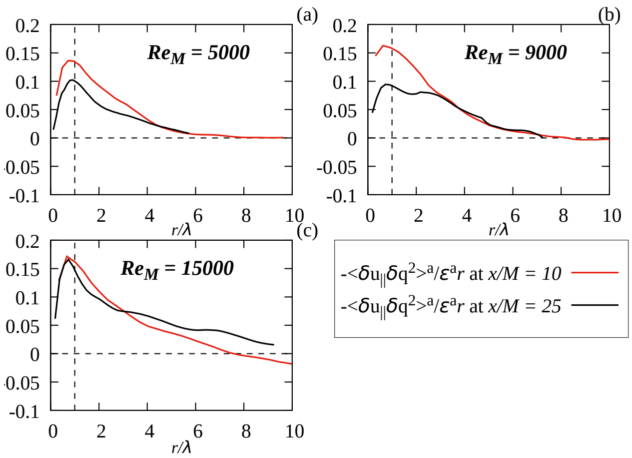

Figure 7. The evolution of the normalized third-order structure functions for the velocity at different positions in cases of (a) $Re_M = 5{,}000$, (b) $Re_M = 9{,}000$ and (c) $Re_M = 15{,}000$.

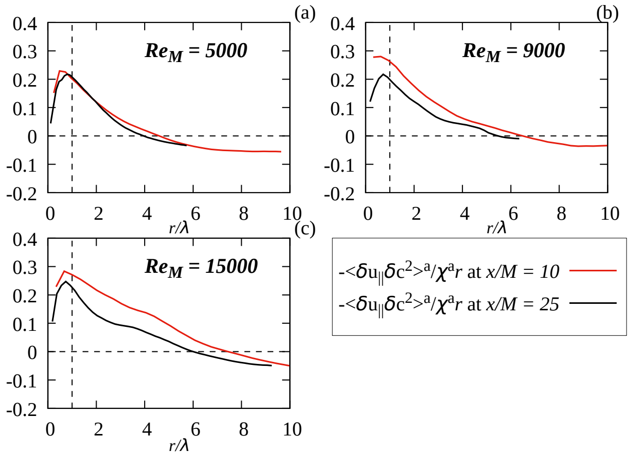

Figure 8. The evolution of the normalized third-order structure functions for the velocity at different positions in cases of (a) $Re_M = 5{,}000$, (b) $Re_M = 9{,}000$ and (c) $Re_M = 15{,}000$.

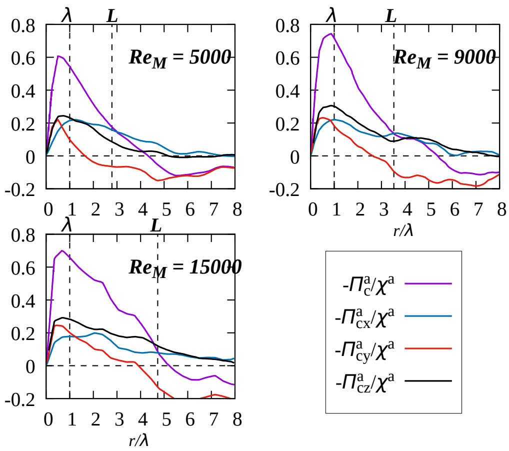

Figure 9. The components of $-\Pi_c^a/\chi^a$ in three directions in cases of (a) $Re_M = 5{,}000$, (b) $Re_M = 9{,}000$ and (c) $Re_M = 15{,}000$.

In order to further study this issue, we continue to decompose the Π_c into two parts:

$$
\begin{aligned}
-\Pi_{cy} &= -\frac{\partial}{\partial r_y}\langle \delta v \delta c^2\rangle = -\langle \delta c^2 \frac{\partial \delta v}{\partial r_y}\rangle - \langle \frac{\partial \delta c^2}{\partial r_y}\delta v\rangle \\
-\Pi_{cy1} &= -\langle \frac{\partial \delta c^2}{\partial r_y}\delta v\rangle = -\frac{1}{2}\langle \delta c^2 \left(\frac{\partial v'}{\partial y'} + \frac{\partial v}{\partial y}\right)\rangle \\
-\Pi_{cy2} &= -\langle \delta c^2 \frac{\partial \delta v}{\partial r_y}\rangle = -\langle \delta v \delta c \left(\frac{\partial c'}{\partial y'} + \frac{\partial c}{\partial y}\right)\rangle
\end{aligned} \tag{5}
$$

Thus, we further decomposed Π_{cy} as shown in Eq. 5. Figure 10 shows the components of $-\Pi_{cy}^a/\chi^a$ at $x/M = 10$ in case of $Re_M = 5{,}000$. It illustrates that $-\Pi_{cy1}^a$ gradually becomes constant while $-\Pi_{cy2}^a$ remains relatively large and maintains the same evolution trend as $-\Pi_{cy}^a$. Therefore, it can be concluded that the vertical flux of the partial derivative of scalar variance $-\Pi_{cy2}^a = \langle \left(\partial \delta c^2/\partial r_y\right) \delta v^a\rangle$ induces the inverse cascade phenomenon for scalar at large scales.

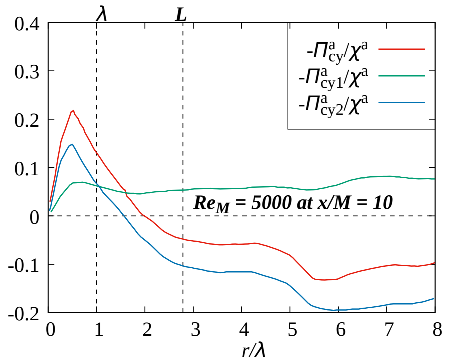

Figure 10. The components of $-\Pi^{a}_{cy}/\chi^{a}$ in case of $Re_M = 5{,}000$ at $x/M = 10$.

CONCLUSIONS

An investigation of the inter-scale scalar transport is conducted based on the DNS data of grid-generated turbulence. The results reveal that the y component of the non-linear transfer term Π_c, which is identical to the direction of the mean scalar gradient, induces the inverse cascade phenomenon for scalar when the scale is large.

ACKNOWLEDGEMENT

The numerical simulations were conducted at Institute of Fluid Science, Tohoku University and and the Earth Simulator Center (JAMSTEC). Part of this research was supported by KAKENHI No.20K04264.

REFERENCES

Gomes-Fernandes, R., Ganapathisubramani, B. and Vassilicos, J.C., 2015, "The energy cascade in near-field nonhomogeneous non-isotropic turbulence", *Journal of Fluid Mechanics*, Vol. 771, pp. 676 - 705.

Meldi, M. and Vassilicos, J.C., 2021, "Structure-function equations for scalars", *Physics of Fluids*, Vol. 14, pp. 1745 – 1756.

Gomes-Fernandes, R., Ganapathisubramani, B. and Vassilicos, J.C., 2015, "Analysis of lundgren's matched asymptotic expansion approach to the karman-howarth equation using the eddy damped quasinormal markovian turbulence closure", *Physical Review Fluids*, Vol. 6, pp. 064602.

Obligado, M. and Vassilicos, J.C., 2019, "The non-equilibrium part of the inertial range in decaying homogeneous turbulence", *Europhysics Letters*, Vol. 127, pp. 64004.

Portela, F.A., Papadakis, G. and Vassilicos, J.C., 2017, "The turbulence cascade in the near wake of a square prism", *Journal of Fluid Mechanics*, Vol. 825, pp. 315 – 352.

Simmons, L. and Salter, C., 1934, "Experimental investigation and analysis of the velocity variations in turbulent flow", *Proceedings of the Royal Society of London*, Vol. 145, pp. 212 – 234.

Yasuda, T. and Vassilicos, J.C., 2018, "Spatio-temporal intermittency of the turbulent energy cascade", *Journal of Fluid Mechanics*, Vol. 853, pp. 235 – 252.

Zhou, Y., Nagata, K., Sakai, Y., Watanabe, T., Ito, Y. and Hayase, T., 2020, "Energy transfer in turbulent flows behind two side-by-side square cylinders, *Journal of Fluid Mechanics*, Vol. 903, pp. 1 - 31.